THE JOURNAL OF PHYSICAL CHEMISTRY C

Article

pubs.acs.org/JPCC

Self-Assembled Patterns and Young's Modulus of Single-Layer Naphthalocyanine Molecules on Ag(111)

Rongting Wu,[†,∥] Linghao Yan,[†,∥] Yanfang Zhang,[†,∥] Junhai Ren,[†] Deliang Bao,[†,‡] Haigang Zhang,[§] Yeliang Wang,[†] Shixuan Du,*[,†] Qing Huan,*[,†] and Hong-Jun Gao[†,‡]

[†]Institute of Physics, Chinese Academy of Sciences, Beijing 100190, China

[‡]University of Chinese Academy of Sciences, Beijing 100049, China

[§]Center for Nanoscale Materials, Argonne National laboratory, Chicago, Illinois 60439, United States

ABSTRACT: Structural and mechanical properties of self-assembled metal-free naphthalocyanine (H_2Nc) films on a Ag(111) surface are studied. Six self-assembled domains are observed by scanning tunneling microscopy (STM). Combining the high-resolution STM images and density functional theory (DFT) based calculations, we found that molecules adsorbed flatly on the substrate by forming six different interlocked square-like unit cells with different lattice parameters. DFT calculations indicated comparable adsorption energies for all the configurations. Six domains with different lattice parameters present different strain states, giving us a possibility to evaluate the Young's modulus of the metal-free naphthalocyanine films on the Ag(111) surface. We found that the Young's modulus of H_2Nc is comparable to those of typical conjugated organic-molecule-based crystals (e.g., naphthalene), providing useful information for future applications when the elastic properties should be concerned.

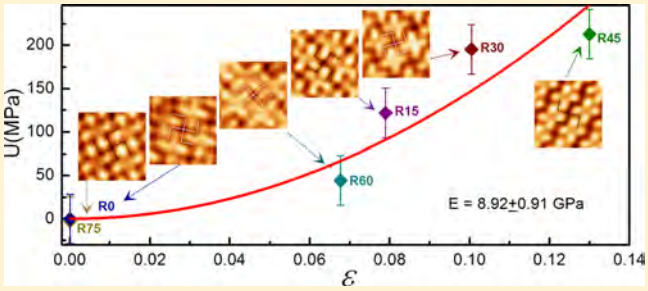

INTRODUCTION

Functional molecules are of great interest in the rapidly growing field of molecular electronics and molecular optics, showing potential applications in electronic and optical devices, such as light-emitting diodes,[1,2] solar cells,[3,4] and switches.[5−8] Because of the fascinating physical properties[9−13] arising from their delocalized π-electronic structures, phthalocyanine (Pc) and its derivatives have been regarded as promising candidates for electronic and optical molecular devices in the last decades.[1,3,14−16] Numerous studies have been carried out about phthalocyanines, such as adsorption,[17−19] structural formation,[17,18,20] and electronic properties[9−11,21] on different substrates. Naphthalocyanines (Ncs), one important class of derivatives of phthalocyanines (Pcs) with an extended delocalized π electron system, show better optical and electronic properties in comparison to Pcs.[12,13] For example, the light-harvesting properties of Ncs are better than those of Pcs since their light absorption matches better with the solar spectrum, which makes them promising candidates for applications in solar cells.[22−24] However, recovery of the physical properties of molecular films from the mechanical deformation is an important issue in practical applications, especially the elastic properties of a molecular monolayer.[25−28] At present, there is little study of the mechanical properties of organic thin films with one monolayer,[29] despite the fact that molecular self-assembly has been extensively investigated on solid surfaces.

In this article, we report on the structural and mechanical properties of self-assembled metal-free naphthalocyanine (H_2Nc) films on a Ag(111) surface at room temperature. Six self-assembled domains are observed during experiment with comparable coverage percentages even after annealing at about 200 °C. From the high-resolution STM images, we found that the molecules adsorb on Ag(111) with the molecular plane parallel to the substrate, further demonstrated by density functional theory (DFT) calculations. The six domains can be divided into two kinds of self-assembly induced chirality,[30] with each chirality containing three domains. DFT calculations indicate a comparable adsorption energy for the six different configurations. By combining the STM measurements and DFT calculations, we evaluated the Young's modulus of the metal-free naphthalocyanine films on the Ag(111) surface, which is comparable to those of typical conjugated organic-molecule-based crystals (e.g., naphthalene).

METHODS

Experimental Section. All experiments were carried out in a homemade ultrahigh vacuum (UHV) scanning tunneling microscope (STM)[31] system with the base pressure better than 2.0×10^{-10} Torr. A single-crystal Ag(111) (roughness <0.03 um, orientation accuracy <0.1°, MaTeck Company) was prepared in vacuum by repeated cycles of Ne^+ sputtering and subsequent annealing at 510 °C until a clean surface was confirmed by STM imaging. 2,3-Naphthalocyanine (Aldrich

Received: February 9, 2015
Revised: March 18, 2015
Published: March 18, 2015

DOI: 10.1021/acs.jpcc.5b01344
J. Phys. Chem. C 2015, 119, 8208−8212

95+%) in powder form was purified by a sublimation process with a homemade Knudsen cell (K-cell) evaporator in high vacuum for 3 days, followed by degassing at 370 °C for 2 h under UHV conditions. The 2,3-naphthalocyanine (H_2Nc) was evaporated at 340 °C with the Ag(111) substrate kept at room temperature. The evaporation rate is about 0.013 ML/min. A monolayer (ML) is defined as the amount of deposited H_2Nc that entirely covers the substrate surface. Electrochemically etched tungsten tips were used as STM tips, and they were further cleaned by several cycles of Ne^+ sputtering and annealing in UHV and checked by STM imaging. All the STM images were taken in constant-current mode, with the bias applied to the sample.

Calculation Details. In order to determine the interaction between the H_2Nc molecules and the substrate, first-principles calculations were carried out based on density functional theory (DFT) with a plane-wave basis set in the Vienna ab initio simulation package (VASP),[32,33] in which projector augmented wave (PAW) potentials were chosen to describe the generalized gradient approximation,[34] with Perdew, Burke, and Ernzernhof (PBE) for exchange-correlation effects. We built all the six supercells of molecular film on the Ag(111) surface based on the lattice parameters from the STM images shown in Figure 2. Considering the calculation limitation, we used a two-layer Ag(111) slab separated by 18 Å vacuum to simulate the substrate of the molecular adsorption. In structural relaxations, silver atoms were fixed in order to improve the calculation efficiency, while all H_2Nc molecules on the surfaces were fully relaxed until the residual forces were smaller than 0.01 eV/Å. The number of atoms in the supercells varies in different configurations due to the different sizes of the supercells. The calculated lattice constant we used for bulk silver was 4.16 Å, which had been proven to be optimal in our previous work.[29] We use Grimme's empirical correction scheme to take into account the van der Waals (vdW) interaction,[35] and the standard values of the calculation parameters are used in these DFT+D/PBE calculations.[36] The adsorption energy for H_2Nc on Ag(111) was defined as $E_a = E_{Nc} + E_{Ag(111)} - E_{Nc/Ag(111)}$.

RESULTS AND DISCUSSION

The top and side views of the relaxed geometrical structures of the H_2Nc molecule calculated by DFT are shown in Figure 1a. The H_2Nc molecule is composed of a phthalocyanine (Pc) skeleton with additional benzene rings attached along the four lobes, increasing the size of each individual molecule by ~0.4 nm. It has a planar geometry (D_{2h}), with a van der Waals diameter of approximately 2 nm.

In submonolayer coverage, neither 2D H_2Nc molecular islands nor monodispersed molecules have been observed. Compared with the reported works of submonolayer coverage of the H_2Nc molecule on a Au(100) surface,[37] these results suggest a weaker interaction between the H_2Nc molecule and the Ag(111) surface. By gradually increasing H_2Nc molecule coverage, a self-assembled monolayer of H_2Nc molecules with multiple domains is observed. We have found six closely packed H_2Nc molecule domains, as shown in Figures 1b, 1c, and 1d. The densely packed lattices in each domain have a specific orientation angle with respect to high-symmetric direction $[1\bar{1}0]$. Here we define the domain, in which one direction of the lattice is along the $[1\bar{1}0]$ direction of Ag(111), as domain R0. For the other five domains, the angles between their lattice orientations and that of the domain R0 in counterclockwise direction are 15°, 30°, 45°, 60°, and 75°; here we define these domains as R15, R30, R45, R60, and R75, respectively.

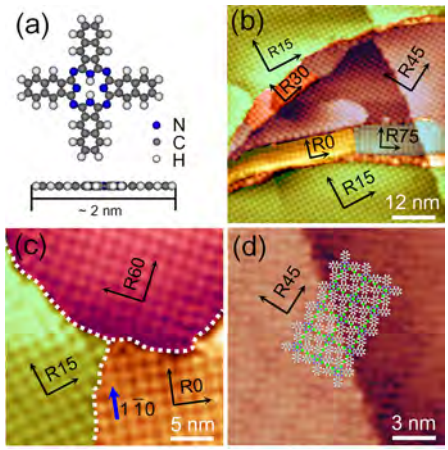

Figure 1. Different domains of a self-assembled H_2Nc molecular monolayer on the Ag(111) surface. (a) Top and side views of H_2Nc molecular structure. (b) STM image of five domains (in different colors) with different lattice directions indicated by the black arrows. (c) STM image of three domains, R0, R15, and R60. R60 is separated with the other two domains by the step edge, and the domain boundary between the domain R0 and R15 is on the upper terrace. The domain boundary is indicated by the white dashed line. (d) STM image shows the monolayer H_2Nc molecules continuously across the step edge. The molecular models are superimposed around the step edge to show the continuity of the molecular layer. The scanning parameters are −2.5 V, 0.1 nA in (b), −1.74 V, 0.1 nA in (c,) and −2.5 V, 0.1 nA in (d), respectively.

Figure 1b shows an STM image including five different domains marked in different colors. In all these domains, the H_2Nc molecules are closely packed and display nearly square lattices. The domain size ranges from tens of nanometers to hundreds of nanometers across several steps. Most of the domain boundaries lie along the step edges, while we could also find domain boundaries on terraces; for example, the domain boundary between domains R0 and R75 is shown in Figure 1b. Figure 1c shows the junction area of three domains, R0, R15, and R60, with the domain boundaries indicated by white dashed lines. We found that the domain R60 is separated from the other two domains by a step edge, while the domain boundary between domain R0 and domain R15 is on the terrace. In the high-resolution STM image [Figure 1d], the domain R45 continuously crosses a step edge, which indicates a stronger intermolecular interaction among H_2Nc molecules than the molecule−substrate interaction. The position and orientation of H_2Nc molecules across the step edge are superimposed by molecular models, and the green dashed lines reveal the unit cells within the R45 domain. All of the six domains are thermally stable up to 200 °C.

Comparing to previous studies of H_2Nc molecular films on graphite[38,39] and other metal substrates,[37,40,41] our work reveals more domains, to the best of our knowledge. Considering the 3-fold symmetry of the Ag(111) surface, the observation of six domains of H_2Nc molecular film indicates a weak but not negligible role of the substrate symmetry on the self-assembly process. By measuring the lattice parameters of the six domains in different areas, we find that the lattice parameters of the molecular monolayer vary a lot, even in the same domain of different areas. Such deformations present different strain states within the molecular film, which gives us the possibility to study

DOI: 10.1021/acs.jpcc.5b01344
J. Phys. Chem. C 2015, 119, 8208−8212

the mechanical properties of the H_2Nc monolayer films on the Ag(111) surface. Here we select six configurations, shown in Figure 2, which enable us to build the commensurate models for the subsequent DFT calculations on the mechanical properties.

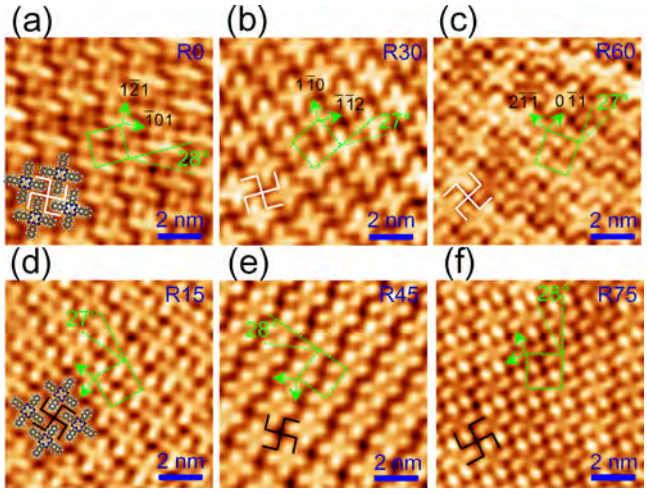

Figure 2. High-resolution STM images of the six different self-assembled domains of H_2Nc molecules on the Ag(111) surface: R0, R15, R30, R45, R60, and R75 in (a), (b), (c), (d), (e), and (f), respectively. The scanning parameters are −1.04 V, 0.1 nA in (a), −1.4 V, 0.1 nA in (b), −1.5 V, 0.1 nA in (c), −1.5 V, 0.1 nA in (d), −2 V, 0.1 nA in (e), and −1.5 V, 0.1 nA in (f).

Figure 2 shows the high-resolution STM images of the six closely packed self-assembled domains. The H_2Nc molecules are represented as crosses with four clearly resolved outer lobes and a depression in the center. The cross represents the position and orientation of the individual molecule within the ad-layer. The H_2Nc molecules are adsorbed flatly on the substrate. The diameter is around 2 nm, which agrees with the calculated van der Waals diameter of the H_2Nc molecule. The H_2Nc molecules are so densely packed that all lobes are interlocked with neighbor molecular lobes just like mechanical gears. The green rhomboid pattern in each image represents the unit cell of the corresponding domains. The unit cells in all of the six domains show similar square shapes, with comparable lattice parameters in the two directions. However, the length of the lattice parameters varies in different domains from 16.1 ± 0.4 to 17.7 ± 0.4 Å, and the angle between the two base vectors ranges from 85 ± 2° to 95 ± 2° (see Table 1 for the detail parameters). This range covers the lattice constant for the H_2Nc molecule on the reported metal surface, such as Au(111)[40,41] and Au(100)[37] (about 17 Å). However, it is a little smaller than the lattice parameters of H_2Nc molecules on graphite[38] (18.5 Å) and larger than the lattice parameters of naphthalocyanines on the inorganic crystals (RbI, KI, KBr, and KCl), which vary from 14.8 to 16.4 Å.[42−44] In our case, the packing density of H_2Nc molecules in different domains in Figure 2 is different, ranging from 0.33 molecules/nm^2 in domain R45 to 0.37 molecules/nm^2 in domain R75. From the atomic resolution STM images on the clean Ag(111) surface before deposition, we could identify the direction of the substrate lattice and thus the relative direction of the adsorbed H_2Nc molecules, as shown in Figure 2.

An interesting feature in the high-resolution STM images (see Figure 2) is that the self-assembly mode of the closely packed molecules can be divided into two chiralities, though a single Nc molecule shows no chirality, which is induced by the surface adsorption.[45,46] For the three domains, R0, R30, and R60 (see Figures 2a, 2b, and 2c, respectively), the H_2Nc molecules are organized in such a way that the nearest four interlocked molecular lobes extend along the clockwise direction. So it leaves a gap between molecules resembling a clockwise (CW) pattern, marked by the white lines, and here we name the chirality "CW". However, for the other three domains, R15, R45, and R75 (see Figures 2d, 2e, and 2f, respectively), the molecules are organized in a different mode; the four nearest interlocked molecular lobes extended along counterclockwise direction, with the gap between molecules resembling a counterclockwise (CCW) pattern, marked by the black lines. Here we name the chirality "CCW".

Table 1. Geometric Parameters and Adsorption Energies of the Six Self-Assembled H_2Nc Molecular Domains in Experiment and DFT Simulation[a]

Structure	R0	R15	R30	R45	R60	R75
A (Å)	16.8±0.4	17.3±0.4	17.3±0.4	17.2±0.4	16.1±0.4	16.5±0.4
B (Å)	16.7±0.4	16.8±0.4	17.2±0.4	17.7±0.4	17.1±0.4	16.6±0.4
Φ (°)	90±2	85±2	93±2	88±2	92±2	92±2
Density (1/nm^2)	0.356±0.16	0.345±0.16	0.337±0.16	0.329±0.16	0.363±0.16	0.365±0.16
Matrix Notation	$\begin{bmatrix}6 & 2\\ 1 & 6\end{bmatrix}$	$\begin{bmatrix}7 & 5\\ -1 & 5\end{bmatrix}$	$\begin{bmatrix}6 & 6\\ -4 & 3\end{bmatrix}$	$\begin{bmatrix}5 & 7\\ -5 & 2\end{bmatrix}$	$\begin{bmatrix}5 & -1\\ 4 & 7\end{bmatrix}$	$\begin{bmatrix}6 & 1\\ 2 & 6\end{bmatrix}$
E_a (eV)	6.113	6.397	6.303	6.565	6.613	6.105
h_i (Å)	3.09	3.03	3.04	3.01	3.01	3.08

[a]The data in the gray background are obtained from the experiments, while those in the orange background are obtained from the DFT calculations.

Using the measured intermolecular distances in different self-assembled domains (shown in Table 1 with gray background), together with the orientation of unit cells and that of a single molecule referring to the orientation of the Ag(111) surface, we built six different commensurate structure models with one molecule in each unit cell, and the matrix notations are presented in Table 1. DFT calculations show that the adsorption energies of the six configurations are comparable (see Table 1), lying in the range of 6.1−6.6 eV, and the distance between molecules and substrates is approximately 3 Å for all configurations. These data show good agreement with the coexistence of the six domains on an annealed sample.

Six domains with lattice parameters varying from 16.1 to 17.7 Å can be regarded as six different strain states of the molecular film. A previous report shows that the Young's modulus is related to the energies and strains of molecular layers at different strain states.[29] The stress−strain relationship of an organic thin film could be approximated as a 2D isotropic system with a strain energy density $U = [E(1 - \upsilon - 1/2\upsilon^2)/(1 - 2\upsilon)]\varepsilon^2$, where E is the Young's modulus, υ the Poisson's ratio, and ε the strain.[47,48] The Poisson's ratio we used for our calculation is 0.3, which is the average value of organic molecular films;[47,49] thus this equation could be further simplified as $U = 1.6375E\varepsilon^2$. Small changes around the average value 0.3 will not change the parameter A too much from 1.6375; for example, when υ changes from 0.25 to 0.35, the $A = (1 - \upsilon - 1/2\upsilon^2)/(1-2\upsilon)$ changes from 1.4375 to 1.9625, resulting in about ±15% variation of the Young's modulus around $E_{0.3}$. The strain ε can be determined by $\varepsilon(i,j) = (S_i^{1/2} -$

DOI: 10.1021/acs.jpcc.5b01344
J. Phys. Chem. C 2015, 119, 8208−8212

$S_j^{1/2})/S_i^{1/2}$, where i and j denote the different structures in the six observed domains and S_i and S_j describe the areas of one molecule in structure i and structure j. The strain energy density U can be evaluated as $U(i,j) = E_{ai}/S_ih_i - E_{aj}/S_jh_j$, where h_i is the thickness of the molecular film on the Ag(111) surface and E_{ai} and E_{aj} are the adsorption energy per molecule in structure i and structure j, respectively.

The strain energy density (U) and strain (ε) for each configuration (R0 ~ R75) shown in Figure 2 can be independently evaluated from our STM measurements and theoretical calculations. By using the formula described above with the data for S (area of one molecule in the observed configuration), E_a (adsorption energy per molecule), and h (thickness of the molecular film), we can easily obtain the values of U and ε of each individual domain.

Figure 3 shows these values and their evolution. Using the formula shown above, $U = 1.6375E\varepsilon^2$, to fit the data in Figure 3,

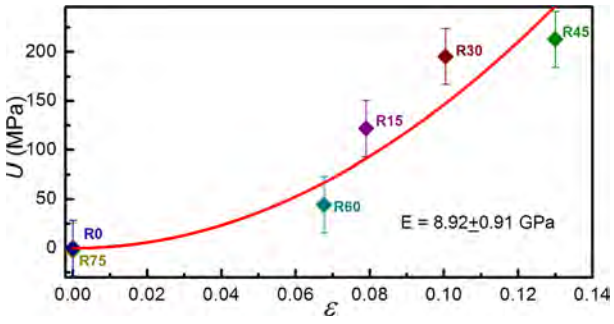

Figure 3. Plot of strain energy density (U) vs strain (ε). The data points from R0 to R75 stand for the calculated values of U and ε of the corresponding domain, and each point is calculated from the domain R0 and itself. The line is a fit to domain R0 through domain R75 resulting in an estimated Young's modulus of 8.92 ± 0.91 GPa. The error of the Young's modulus comes from the standard error when we use a quadratic function to fit the $U-\varepsilon$ data.

we find that a single Young's modulus applies to all configurations and that the value is 8.92 ± 0.91 GPa. This value is comparable with those of typical conjugated organic-molecule-based crystals (e.g., naphthalene and anthracene have Young's modulus of 8.1 and 8.4 GPa, respectively[47]). This is consistent with the fact that the H_2Nc molecules have four naphthalene-like lobes, which provide the main contribution to the interaction between neighboring molecules. The interlocked packing mode limits the dislocation and rotation of the single molecule within the ad-layer, which also contributes to the elastic properties of the molecular film.

CONCLUSION

The self-assembled configurations and the mechanical properties of H_2Nc molecules on a Ag(111) surface were investigated by STM measurements combined with DFT calculations. The H_2Nc molecules adsorbed flatly on the substrate. Six different self-assembled H_2Nc molecular domains were observed. High-resolution STM images of the six domains show that the cross-like shaped molecules are packed with neighboring lobes interlocked with each other. This pattern shows two kinds of self-assembly-induced chirality within six domains, with the gaps in between molecules resembling the CW and CCW patterns in different chiralities. Atomic resolution STM images of the Ag(111) surface obtained before H_2Nc molecule deposition were utilized to determine the single-molecule and the unit cell orientations of self-assembled patterns, together with the lattice constants obtained during experiment, and structure models of the six configurations were provided. By combining the STM measurements and theoretical calculations, we obtained the Young's modulus of the metal-free naphthalocyanine films on the Ag(111) surface.

AUTHOR INFORMATION

Corresponding Authors

*E-mail: sxdu@iphy.ac.cn

*E-mail: huanq@iphy.ac.cn.

Author Contributions

‖Rongting Wu, Linghao Yan, and Yanfang Zhang contributed equally to this work.

Notes

The authors declare no competing financial interest.

ACKNOWLEDGMENTS

The authors thank Werner A. Hofer and Sokrate Pantelides for fruitful discussions. This work was financially supported by the NSFC (Nos. 61390501, 51325204, and 11204361), National "973" program (Nos. 2011CB808401, and 2011CB921702) of China, National Key Scientific Instrument and Equipment Development Project of China (No. 2013YQ1203451), National Supercomputing Center in Tianjin, and the CAS.

REFERENCES

(1) Wang, S.; Liu, Y.; Huang, X.; Yu, G.; Zhu, D. Phthalocyanine Monolayer-Modified Gold Substrates as Efficient Anodes for Organic Light-Emitting Diodes. *J. Phys. Chem. B* **2003**, *107*, 12639−12642.

(2) Forrest, S. R. The Path to Ubiquitous and Low-Cost Organic Electronic Appliances on Plastic. *Nature* **2004**, *428*, 911−918.

(3) Koeppe, R.; Sariciftci, N. S.; Troshin, P. A.; Lyubovskaya, R. N. Complexation of Pyrrolidinofullerenes and Zinc-Phthalocyanine in a Bilayer Organic Solar Cell Structure. *Appl. Phys. Lett.* **2005**, *87*, 244102−244101.

(4) Tan, Q.; Zhang, X.; Mao, L.; Xin, G.; Zhang, S. Novel Zinc Porphyrin Sensitizers for Dye-Sensitized Solar Cells: Synthesis and Spectral, Electrochemical, and Photovoltaic Properties. *J. Mol. Struct.* **2013**, *1035*, 400−406.

(5) Gao, H. J.; Sohlberg, K.; Xue, Z. Q.; Chen, H. Y.; Hou, S. M.; Ma, L. P.; Fang, X. W.; Pang, S. J.; Pennycook, S. J. Reversible, Nanometer-Scale Conductance Transitions in an Organic Complex. *Phys. Rev. Lett.* **2000**, *84*, 1780−1783.

(6) Moresco, F.; Meyer, G.; Rieder, K.-H.; Tang, H.; Gourdon, A.; Joachim, C. Conformational Changes of Single Molecules Induced by Scanning Tunneling Microscopy Manipulation: A Route to Molecular Switching. *Phys. Rev. Lett.* **2001**, *86*, 672−675.

(7) Emberly, E. G.; Kirczenow, G. The Smallest Molecular Switch. *Phys. Rev. Lett.* **2003**, *91*, 188301.

(8) Gao, H. J.; Gao, L. Scanning Tunneling Microscopy of Functional Nanostructures on Solid Surfaces: Manipulation, Self-Assembly, and Applications. *Prog. Surf. Sci.* **2010**, *85*, 28−91.

(9) Hipps, K. W.; Barlow, D. E.; Mazur, U. Orbital Mediated Tunneling in Vanadyl Phthalocyanine Observed in Both Tunnel Diode and Stm Environments. *J. Phys. Chem. B* **2000**, *104*, 2444−2447.

(10) Barlow, D. E.; Hipps, K. W. A Scanning Tunneling Microscopy and Spectroscopy Study of Vanadyl Phthalocyanine on Au(111): The Effect of Oxygen Binding and Orbital Mediated Tunneling on the Apparent Corrugation. *J. Phys. Chem. B* **2000**, *104*, 5993−6000.

(11) Lu, X.; Hipps, K. W.; Wang, X. D.; Mazur, U. Scanning Tunneling Microscopy of Metal Phthalocyanines: D7 and D9 Cases. *J. Am. Chem. Soc.* **1996**, *118*, 7197−7202.

(12) Hanack, M.; Schneider, T.; Barthel, M.; Shirk, J. S.; Flom, S. R.; Pong, R. G. S. Indium Phthalocyanines and Naphthalocyanines for Optical Limiting. *Coord. Chem. Rev.* **2001**, *219−221*, 235−258.

DOI: 10.1021/acs.jpcc.5b01344
J. Phys. Chem. C 2015, 119, 8208−8212

(13) El-Khouly, M. E.; Gutierrez, A. M.; Sastre-Santos, A.; Fernandez-Lazaro, F.; Fukuzumi, S. Light Harvesting Zinc Naphthalocyanine-Perylenediimide Supramolecular Dyads: Long-Lived Charge-Separated States in Nonpolar Media. *Phys. Chem. Chem. Phys.* **2012**, *14*, 3612−3621.
(14) Peumans, P.; Forrest, S. R. Very-High-Efficiency Double-Heterostructure Copper Phthalocyanine/C-60 Photovoltaic Cells. *Appl. Phys. Lett.* **2001**, *79*, 126−128.
(15) Crone, B.; Dodabalapur, A.; Lin, Y. Y.; Filas, R. W.; Bao, Z.; LaDuca, A.; Sarpeshkar, R.; Katz, H. E.; Li, W. Large-Scale Complementary Integrated Circuits Based on Organic Transistors. *Nature* **2000**, *403*, 521−523.
(16) Peumans, P.; Yakimov, A.; Forrest, S. R. Small Molecular Weight Organic Thin-Film Photodetectors and Solar Cells. *J. Appl. Phys.* **2003**, *93*, 3693−3723.
(17) Gopakumar, T. G.; Lackinger, M.; Hackert, M.; Müller, F.; Hietschold, M. Adsorption of Palladium Phthalocyanine on Graphite: Stm and Leed Study. *J. Phys. Chem. B* **2004**, *108*, 7839−7843.
(18) Suto, K.; Yoshimoto, S.; Itaya, K. Two-Dimensional Self-Organization of Phthalocyanine and Porphyrin: Dependence on the Crystallographic Orientation of Au. *J. Am. Chem. Soc.* **2003**, *125*, 14976−14977.
(19) Nilson, K.; Åhlund, J.; Brena, B.; Göthelid, E.; Schiessling, J.; Mårtensson, N.; Puglia, C. Scanning Tunneling Microscopy Study of Metal-Free Phthalocyanine Monolayer Structures on Graphite. *J. Chem. Phys.* **2007**, *127*, 114702.
(20) Ogunrinde, A.; Hipps, K. W.; Scudiero, L. A Scanning Tunneling Microscopy Study of Self-Assembled Nickel(Ii) Octaethylporphyrin Deposited from Solutions on Hopg. *Langmuir* **2006**, *22*, 5697−5701.
(21) Zhang, Y. Y.; Du, S. X.; Gao, H. J. Binding Configuration, Electronic Structure, and Magnetic Properties of Metal Phthalocyanines on a Au(111) Surface Studied with *Ab Initio* Calculations. *Phys. Rev. B* **2011**, *84*, 125446.
(22) Kobayashi, N.; Nakajima, S.; Ogata, H.; Fukuda, T. Synthesis, Spectroscopy, and Electrochemistry of Tetra-Tert-Butylated Tetraazaporphyrins, Phthalocyanines, Naphthalocyanines, and Anthracocyanines, Together with Molecular Orbital Calculations. *Chem.—Eur. J.* **2004**, *10*, 6294−6312.
(23) Lim, B.; Margulis, G. Y.; Yum, J.-H.; Unger, E. L.; Hardin, B. E.; Grätzel, M.; McGehee, M. D.; Sellinger, A. Silicon-Naphthalo/Phthalocyanine-Hybrid Sensitizer for Efficient Red Response in Dye-Sensitized Solar Cells. *Org. Lett.* **2013**, *15*, 784−787.
(24) Pandey, R.; Kerner, R. A.; Menke, S. M.; Holst, J.; Josyula, K. V. B.; Holmes, R. J. Tin Naphthalocyanine Complexes for Infrared Absorption in Organic Photovoltaic Cells. *Org. Electron.* **2013**, *14*, 804−808.
(25) Kisielowski, C.; Krüger, J.; Ruvimov, S.; Suski, T.; Ager, J. W.; Jones, E.; Liliental-Weber, Z.; Rubin, M.; Weber, E. R.; Bremser, M. D.; et al. Strain-Related Phenomena in Gan Thin Films. *Phys. Rev. B* **1996**, *54*, 17745−17753.
(26) Rogers, J. A.; Someya, T.; Huang, Y. Materials and Mechanics for Stretchable Electronics. *Science* **2010**, *327*, 1603−1607.
(27) Mueggenburg, K. E.; Lin, X.-M.; Goldsmith, R. H.; Jaeger, H. M. Elastic Membranes of Close-Packed Nanoparticle Arrays. *Nat. Mater.* **2007**, *6*, 656−660.
(28) Rieger, W.; Metzger, T.; Angerer, H.; Dimitrov, R.; Ambacher, O.; Stutzmann, M. Influence of Substrate-Induced Biaxial Compressive Stress on the Optical Properties of Thin Gan Films. *Appl. Phys. Lett.* **1996**, *68*, 970−972.
(29) Cun, H. Y.; Wang, Y. L.; Du, S. X.; Zhang, L.; Zhang, L. Z.; Yang, B.; He, X. B.; Wang, Y.; Zhu, X. Y.; Yuan, Q. Z.; et al. Tuning Structural and Mechanical Properties of Two-Dimensional Molecular Crystals: The Roles of Carbon Side Chains. *Nano Lett.* **2012**, *12*, 1229−1234.
(30) Ernst, K.-H. Molecular Chirality at Surfaces. *Phys. Status Solidi B* **2012**, *249*, 2057−2088.
(31) Stipe, B. C.; Rezaei, M. A.; Ho, W. A Variable-Temperature Scanning Tunneling Microscope Capable of Single-Molecule Vibrational Spectroscopy. *Rev. Sci. Instrum.* **1999**, *70*, 137−143.
(32) Vanderbilt, D. Soft Self-Consistent Pseudopotentials in a Generalized Eigenvalue Formalism. *Phys. Rev. B* **1990**, *41*, 7892−7895.
(33) Kresse, G.; Furthmuller, J. Efficient Iterative Schemes for Ab Initio Total-Energy Calculations Using a Plane-Wave Basis Set. *Phys. Rev. B* **1996**, *54*, 11169−11186.
(34) Perdew, J. P.; Chevary, J. A.; Vosko, S. H.; Jackson, K. A.; Pederson, M. R.; Singh, D. J.; Fiolhais, C. Atoms, Molecules, Solids, and Surfaces - Applications of the Generalized Gradient Approximation for Exchange and Correlation. *Phys. Rev. B* **1992**, *46*, 6671−6687.
(35) Grimme, S. Semiempirical Gga-Type Density Functional Constructed with a Long-Range Dispersion Correction. *J. Comput. Chem.* **2006**, *27*, 1787−1799.
(36) Bucko, T.; Hafner, J.; Lebegue, S.; Angyan, J. G. Improved Description of the Structure of Molecular and Layered Crystals: Ab Initio Dft Calculations with Van Der Waals Corrections. *J. Phys. Chem. A* **2010**, *114*, 11814−11824.
(37) Mehring, P.; Beimborn, A.; Luhr, T.; Westphal, C. Metal-Free Naphthalocyanine Structures on Au(100) at Submonolayer Coverage. *J. Phys. Chem. C* **2012**, *116*, 12819−12823.
(38) Gopakumar, T. G.; Muller, F.; Hietschold, M. Scanning Tunneling Microscopy and Scanning Tunneling Spectroscopy Studies of Planar and Nonplanar Naphthalocyanines on Graphite (0001). Part 1: Effect of Nonplanarity on the Adlayer Structure and Voltage-Induced Flipping of Nonplanar Tin-Naphthalocyanine. *J. Phys. Chem. B* **2006**, *110*, 6051−6059.
(39) Gopakumar, T. G.; Muller, F.; Hietschold, M. Scanning Tunneling Microscopy and Scanning Tunneling Spectroscopy Studies of Planar and Nonplanar Naphthalocyanine on Graphite(0001). Part 2: Tip-Sample Distance-Dependent I-V Spectroscopy. *J. Phys. Chem. B* **2006**, *110*, 6060−6065.
(40) Wiggins, B.; Hipps, K. W. Investigation of Metal Free Naphthalocyanine Vapor Deposited on Au(111). *J. Phys. Chem. C* **2014**, *118*, 4222−4230.
(41) Pham, T. A.; Song, F.; Stohr, M. Supramolecular Self-Assembly of Metal- Free Naphthalocyanine on Au(111). *Phys. Chem. Chem. Phys.* **2014**, *16*, 8881−8885.
(42) Yanagi, H.; Ashida, M.; Elbe, J.; Woehrle, D. Crystal Growth and Molecular Orientation of Vanadylnaphthalocyanine in Thin Films. *J. Phys. Chem.* **1990**, *94*, 7056−7061.
(43) Yanagi, H.; Kouzeki, T.; Ashida, M. Epitaxial-Growth of Naphthalocyanine Thin-Films Vacuum-Deposited on Alkali-Halides. *J. Appl. Phys.* **1993**, *73*, 3812−3819.
(44) Tada, H.; Morioka, T.; Koma, A. Epitaxial-Growth of Ultrathin Vanadyl-Naphthalocyanine Films on Rbi, Ki and Kbr. *J. Phys.: Condens. Matter* **1994**, *6*, 1881−1892.
(45) Yang, K.; Liu, L.; Zhang, L.; Xiao, W.; Fei, X.; Chen, H.; Du, S.; Ernst, K.-H.; Gao, H.-J. Reversible Achiral-to-Chiral Switching of Single Mn−Phthalocyanine Molecules by Thermal Hydrogenation and Inelastic Electron Tunneling Dehydrogenation. *ACS Nano* **2014**, *8*, 2246−2251.
(46) Yang, B.; Wang, Y.; Cun, H.; Du, S.; Xu, M.; Wang, Y.; Ernst, K.-H.; Gao, H.-J. Direct Observation of Enantiospecific Substitution in a Two-Dimensional Chiral Phase Transition. *J. Am. Chem. Soc.* **2010**, *132*, 10440−10444.
(47) Simmons, G.; Wang, H. *Single Crystal Elastic Constants and Calculated Aggregate Properties: A Handbook*; the Mit Press: Cambridge. U.K., 1971; pp133−311.
(48) Sun, D.; Kim, D.-H.; Le, D.; Borck, Ø.; Berland, K.; Kim, K.; Lu, W.; Zhu, Y.; Luo, M.; Wyrick, J.; et al. Effective Elastic Properties of a Van Der Waals Molecular Monolayer at a Metal Surface. *Phys. Rev. B* **2010**, *82*, 201410.
(49) Roberts, R. J.; Rowe, R. C.; York, P. The Relationship between Young's Modulus of Elasticity of Organic Solids and Their Molecular Structure. *Powder Technol.* **1991**, *65*, 139−146.

DOI: 10.1021/acs.jpcc.5b01344
J. Phys. Chem. C 2015, 119, 8208−8212